# Molecular Orientation in Poly(4-oxybenzoate-*co*-1,4-phenylene isophthalate) by Slow-Magic-Angle-Spinning DECODER NMR

**M.-Y. Liao and G. C. Rutledge***

*Department of Chemical Engineering, Massachusetts Institute of Technology, Cambridge, Massachusetts 02139*

*Received June 24, 1997; Revised Manuscript Received September 3, 1997*[⊗]

ABSTRACT: Slow-magic-angle-spinning DECODER NMR based on the anisotropy of chemical shift tensors is used to determine molecular-level orientation in three samples of poly(4-oxybenzoate-*co*-1,4-phenylene isophthalate) of comparable composition but different process histories. The two-dimensional NMR line shapes are sufficiently resolved to show quantitative differences in the degree of orientation for powder, melt-extruded monofilament, and high-speed melt-spun fiber of the wholly aromatic liquid crystal polymer produced from an approximately equimolar mixture of 4-hydroxybenzoic acid, hydroquinone, and isophthalic acid. By direct comparison of calculated and experimental NMR line shapes, the full orientation distribution functions for all repeat units were determined and found to be consistent with a combination of isotropic and anisotropic components. Multiple reorientation angles are used to confirm the proposed molecular orientation distributions. The results indicate a high degree of orientation in the melt-spun fiber, a lesser degree of orientation in the melt-extruded monofilament, and isotropic orientation in the powder sample. Legendre polynomial expansions up to order $n = 14$ were estimated.

## Introduction

The macroscopic properties of a polymeric material are functions of the microscopic structure which forms during processing. Of particular interest is the extent of molecular orientation, which plays an important role in determining mechanical properties.[1] Most wholly aromatic polyesters are main chain liquid crystal polymers capable of being processed from melt or solution to form high-strength, high-modulus fibers and high-performance engineering materials, due to the high degree of molecular orientation attainable.[2] The homopolyesters poly(4-hydroxybenzoic acid) and poly(1,4-phenylene terephthalate) decompose before they reach their melting points and are difficult to dissolve in conventional solvents. Processability in this family of polymers has been accomplished by the use of molecular strategies to disrupt intermolecular packing regularity with minimal loss of chain rigidity and the outstanding tensile properties typically resulting therefrom. One strategy is the copolymerization of rigid monomers of different sizes to frustrate crystallization, the best known example being the copolyesters of 4-hydroxybenzoic acid (HBA) and 2-hydroxy-6-naphthoic acid (HNA), which are produced by Hoechst-Celanese under the trade name Vectra and have been the subject of intensive study for the last decade. A second strategy involves inclusion of nonlinear segments with a meta aromatic linkage into the chain backbone in varying amounts, trading off rodlike behavior for processability and improvements in compressive properties. The terpolyesters of HBA, isophthalic acid (IA), and hydroquinone (HQ) are examples of this approach, which has also attracted considerable attention.[3−9] A third popular strategy involves the use of flexible aliphatic spacers in the main chain, which imparts processability at the cost of both rigidity and rodlike persistence. The materials which are the subject of this report belong to the second strategy. We employ the nomenclature HIQ-x, where $x$ indicates the molar ratio of components HBA:IA:HQ = $x$:(1 − $x$)/2:(1 − $x$)/2 in the terpolyester. The HIQ samples are of interest because the intrinsic rigidity of the polymer chain gives rise to a thermotropic liquid crystal phase over a broad range of composition and temperature.[8,9] This facilitates the attainment of high degrees of molecular orientation on the time scale of conventional processing. In this work, we focus on samples of HIQ-35, which either are in the form of as-synthesized powder or have been melt-processed at different rates to achieve varying degrees of molecular extension.

The orientation distributions of oriented or partially-oriented materials have been determined by numerous methods, the most common being birefringence,[10] wide-angle X-ray scattering (WAXS),[11] and nuclear magnetic resonance (NMR) measurements.[12] Birefringence measurements, like absorption spectroscopy, permit interpretation in terms of orientation distributions of specific chemical units, but estimation of only the first two moments of the orientation distribution function is possible by these methods. Except in cases of relatively low degrees of orientation, this is inadequate to describe the orientation distribution function. WAXS measurements have been used extensively to measure molecular orientation in polymers but are mainly useful when describing the orientation of crystalline phases. Previous attempts have been made to quantify orientation in liquid crystal polymers by evaluating the azimuthal spread of intensity about selected reflections in the experimental fiber pattern. For rodlike chains such as the HBA−HNA copolymers, meridional reflections have been used to estimate the orientation distribution associated with single-chain "scattering units" having a correlation length of approximately 10 repeat units.[13,14] In studies of HIQ samples, equatorial reflections were used due to the low intensity of the more relevant meridional reflections.[15,16] However, the WAXS method is complicated by the fact that the azimuthal spread of intensity reflects a convolution of both orientational disorder and structural disorder; at high degree of orientation, the spreading of intensity due to these two contributions can be comparable and leads to erroneous results unless properly separated.[17] Such separation is greatly complicated by the lack of a precise knowledge of the "scattering unit", since both intramolecular conformation and interchain packing correlations must

[⊗] Abstract published in *Advance ACS Abstracts,* November 1, 1997.

S0024-9297(97)00927-3 CCC: $14.00 

in general be taken into account. NMR techniques have several advantages for this type of study: the measured intensity, and thus also the orientation distribution, can be identified with distinct molecular species; both the crystalline and noncrystalline components may be observed; in principle, the full orientation distribution and all its moments are accessible.

For decades, molecular orientation in polymers has been determined by broad line NMR line shape analysis of the dipolar interaction.[18] This method has also been applied previously to the investigation of aromatic polyesters, including HIQ-35, by Ward and co-workers.[19,20] However, due to the restrictions on acquisition of the FID at short times, where the technique is most sensitive to higher order moments of the orientation distribution, only the first few moments are reliably obtained by broad line NMR line shape measurements. More recent methods for extracting molecular orientation information in polymer solids from one dimensional line shape analysis have taken advantage of the angular dependence of the $^2$H quadrupolar interaction,[21−23] for example in polyethylene, or anisotropic chemical shift ($^{13}$C) frequencies,[24,25] for example in poly(methyl methacrylate). However, for most polymers these methods require isotopic enrichment in order to attain adequate sensitivity and to avoid problems of spectral overlap, in the case of anisotropic chemical shift spectra. More recently, advancements in multidimensional solid-state NMR techniques have permitted the extraction of molecular order information based on either the calculation of the intensities of 2D side bands using rotor synchronization CPMAS, as described by Harbison et al.,[26,27] or the simulation of 2D line shapes obtained by macroscopic reorientation and detection during two different time periods, as described by Henrichs.[28] The later technique has been elaborated for polymers by Spiess and co-workers,[29,30] who proposed the acronym DECODER (*d*irection *e*xchange with *c*orrelation for *o*rientation *d*istribution *e*valuation and *r*econstruction) NMR. The 2D correlation technique has been applied to the line shapes arising from the orientation dependence of the anisotropic chemical shift tensor,[30] the quadrupolar interaction tensor,[29] and, in the case of selectively $^{13}$C labeled samples, the dipolar coupling tensor.[31] In its original implementation, reorientation was achieved by mechanically flipping the sample between two static orientations with respect to the magnetic field. Recently, Lewis et al.[32] demonstrated a variant of DECODER using slow continuous rotation of the sample about the magic angle using a conventional CPMAS probe; this variant is simpler to implement than the static mechanical flip. This new method, which for the sake of brevity we denote here as SMAS−DECODER (slow-magic-angle-spinning DECODER), has the advantages of simplicity of probe construction and capability for fast reorientation to avoid problems in materials exhibiting short longitudinal relaxation times and spin diffusion. Here, we describe our use of the SMAS−DECODER method to measure the molecular orientation of different samples of HIQ (with approximately 35 ± 5% of HBA) having different process histories and covering a broad range of molecular orientation.

## Slow-Magic-Angle-Spinning DECODER

The DECODER experiment correlates the resonance frequency measured before and after a macroscopic reorientation of the sample, which allows one to determine the orientation distribution of the chemical shift tensors (the so-called principal axis frame of reference) with respect to the magnetic field. Knowing the orientation of the sample itself in the magnetic field and the orientation of the principal axes of the interaction tensor with respect to the structure of the molecule, or some short architectural subunit of the polymer chain (e.g. repeat unit), one can determine the orientation distribution of the architectural subunits within the sample, often referred to as the "molecular orientation". The important coordinate systems involved in the SMAS−DECODER experiment are illustrated schematically in Figure 1 and have been described in detail previously.[12,29,30,32] The laboratory frame (LF) refers to the direction of the static magnetic field and the rotor frame (RF) refers to the direction of the rotor axis, both of which are prescribed during the experimental setup. The director frame (DF) is chosen to correspond to the axes of orientation symmetry in the sample, based on knowledge of the deformation and flow history of the material. The molecular frame (MF) refers to a user-defined reference direction in the architectural subunits chosen to describe the molecular orientation. The principal axis system (PAS) denotes the reference frame of the interaction tensor, which in our case corresponds to the chemical shift anisotropy (CSA) tensors of each carbon site, with respect to the architectural subunit.

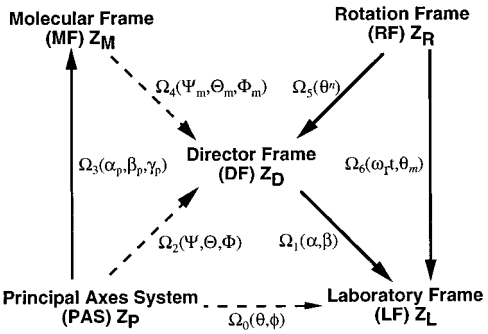


**Figure 1.** Relative orientation (Euler angles) between different reference frames involved in the SMAS−DECODER experiment.

In the $^{13}$C CSA version of the DECODER experiment, the 2D-NMR line shapes are based on the orientation distribution function $P(\theta,\phi)$ of the PAS in the LF and the orientation dependent frequency $\omega(\theta, \phi)$ for each carbon site, where $\theta$ and $\phi$ are the polar angles of the magnetic field $\mathbf{B}_0$ with respect to the anisotropic chemical shift tensors in the PAS.

$$\omega(\theta,\phi) = \omega_{iso} + \frac{\Delta}{2}[3\cos^2\theta - 1 - \eta \sin^2 \theta \cos(2\phi)] \quad (1)$$

$\omega_{iso} = \omega_0\sigma_{iso}$ is the isotropic chemical shift, where $\sigma_{iso} = (\sigma_x + \sigma_y + \sigma_z)/3$ is a function of the principal values $\sigma_{i=x,y,z}$ of the chemical shift tensor, and $\omega_i = \omega_0\sigma_i$. $\omega_0$ is the Larmor frequency. The chemical shift anisotropy parameter $\Delta$ and the asymmetry parameter $\eta$ are functions of the principal values and are defined as $\Delta = \omega_z - \omega_{iso}$ and $\eta = (\omega_y - \omega_x)/\Delta$.[12,33−35] Given knowledge of the CSA tensors, the DECODER 2D-NMR line shapes can be calculated for any $P(\theta,\phi)$ as follows:

$$S(\tilde{\omega}_1,\tilde{\omega}_2) = \frac{\int_0^{2\pi}\int_0^{\pi} P(\theta,\phi)\delta(\tilde{\omega}_1 - \omega(\theta,\phi)|_1)\delta(\tilde{\omega}_2 - \omega(\theta,\phi)|_2)\sin\theta\,\mathrm{d}\theta\,\mathrm{d}\phi}{\int_0^{2\pi}\int_0^{\pi} P(\theta,\phi)\sin\theta\,\mathrm{d}\theta\,\mathrm{d}\phi} \quad (2)$$

where $\omega(\theta, \phi)|_i$ is the frequency spectrum observed before ($i = 1$) or after ($i = 2$) the sample reorientation. As described below, spectral overlap as well as nonzero asymmetry parameters preclude direct reconstruction of the orientation distribution from $S(\tilde{\omega}_1,\tilde{\omega}_2)$. In practice, we initially assume a distribution $P(\Psi_M,\Theta_M,\Phi_M)$ and compute $\omega(\theta,\phi)|_i = \omega(\alpha,\beta,\Psi,\Theta,\Phi)|_i$ and $P(\alpha_p,\beta_p,\gamma_p,\Psi,\Theta,\Phi)$. The integration is then performed over $\Psi$, $\Theta$, and $\Phi$. The distribution $P(\Psi_M,\Theta_M,\Phi_M)$ is then varied to attain agreement between experimental and simulated $S(\tilde{\omega}_1,\tilde{\omega}_2)$ spectra.

In specifying the orientation distribution function $P(\Psi_M,\Theta_M,\Phi_M)$ we take advantage of the symmetry of the polymer sample. For a collection of fibers exhibiting transverse isotropy, or so-called fiber symmetry, it suffices to describe the orientation distribution function by a distribution in one variable, the azimuthal angle $\Theta_M$ between the *z*-axes of the MF and the DF. For this situation we have assumed a distribution function consisting of a Gaussian distribution in $\sin(\Theta_M)$ for the oriented component of the sample and a uniform distribution for the isotropic component.

$$P(\Theta_M) = \frac{(1-f)}{N_1}\exp\left[-(4\ln 2)\frac{\sin^2(\Theta_M - \Theta_M^0)}{\Delta\Theta_M{}^2}\right] + \frac{f}{N_2} \quad (3)$$

$f$ is the fraction of the isotropic component in the sample. $N_1$ and $N_2$ are normalization factors for each component, so that fractional contributions are expressed on an equal area basis. $\Delta\Theta_M$ is the full width at half-maximum (fwhm) of the Gaussian distribution. $\Theta_M^0$ is the center of the Gaussian distribution. As discussed later, the selection of axes in the MF is somewhat arbitrary, leading to distributions which may be peaked about angles other than $\Theta_M^0 = 0$ degrees, in the general case. However, we have chosen the MF in each instance so that the *z*-axis of the MF is consistent with the expected axis of symmetry for the orientation distribution. We also considered values of $\Theta_M^0$ other than zero in our simulations, but found that values greater than about 10−15° led to spectra which were qualitatively inconsistent with experimental observations. All of the results reported in this work employed $\Theta_M^0 = 0°$. Conventionally, the orientation distribution function $P(\Theta_M)$ of the uniaxial symmetric system is described as a summation of Legendre polynomials, $P_n(\cos\Theta_M)$.[17,36]

$$P(\Theta_M) = \sum_n a_n P_n(\cos\Theta_M) \quad (4)$$

The orthogonality condition for the Legendre polynomials leads to the following expression for the expansion coefficients $a_n$:

$$a_n = \frac{(2n+1)}{4\pi}\langle P_n(\cos\Theta_M)\rangle \quad (5)$$

The orientation distribution in a sample is then characterized by a set of order parameters corresponding to the Legendre polynomial averages $P_n = \langle P_n(\cos\Theta_M)\rangle$.

$$\langle P_n(\cos\Theta_M)\rangle = \frac{\int_0^{\pi/2} P(\Theta_M)P_n(\cos\Theta_M)\sin\Theta_M\,\mathrm{d}\Theta_M}{\int_0^{\pi/2} P(\Theta_M)\sin\Theta_M\,\mathrm{d}\Theta_M} \quad (6)$$

$P_2$ is the well-known Herman's orientation parameter. Higher order terms of the Legendre polynomial series are required to describe accurately orientation distribution functions of high degree of orientation.

## Experimental Section

The experiments were performed on as-polymerized HIQ powder (courtesy of the Textiles Department, University of Leeds) and HIQ melt-extruded monofilament and melt-spun fibers (courtesy of Hoechst Celanese, Summit, NJ), all of which contain about 35 mol % HBA monomer and no isotopic enrichment. The monofilament is ca. 765 $\mu$m in diameter, having a slightly noncircular cross section with ±6% deviation in each principal axis dimension. The fibers are 25 ± 0.5 $\mu$m in diameter. The HIQ powder sample was ground to fine powder without further purification and put into the rotor directly. The HIQ melt-spun fiber and melt-extruded monofilament samples were assembled into bundles and wrapped with Teflon tape. Talc (Aldrich) was used to pack the samples in the rotor and to ensure proper balancing during spinning. The initial orientation $\alpha_0$ of the sample must be estimated from the position of the sample director relative to the mark of the rotor. However, when the sample axes are packed parallel to the rotor axis, accurate knowledge of initial sample position and rotor synchronization is not necessary due to the uniaxial symmetry of the monofilament and fiber samples. Thus for the purposes of this study, misalignment errors were minimized by inserting the oriented sample into the rotor with the fiber axis (DF *z*-axis) parallel to the rotor axis for all measurements.

The experiments were conducted on a home-built spectrometer designed for solid state measurements. The $^{13}C$ and $^{1}H$ resonance frequencies on this system are 67.906 and 270.024 MHz, respectively. Pulse sequence and data acquisition were controlled using the Tecmag LIBRA system. The probe is a standard Chemagnetics 7.5 mm double-resonance magic-angle-spinning probe. The 90 degree pulse length for both channels is 4 $\mu$s. Spinning speed was controlled by the Chemagnetics MAS spin controller unit, which provides a rotor trigger signal to the LIBRA system to achieve rotor-synchronization. The spinning rate was closely monitored and was stable at 100 Hz with fluctuations of less than 1 Hz during each experiment. The SMAS−DECODER pulse sequence is shown in Figure 2. The reorientation angle $\omega_r\tau_m$ was held constant so that the mixing time ($\tau_m - t_1$) varied with the $t_1$ increment. An echo pulse with delay $\tau$ was applied before acquisition to avoid the receiver dead time. The FIDs were collected with a cross-polarization time of 2 ms and a recycle delay of 3 s. Most of the 2D data sets were measured using a dwell time of 20 $\mu$s in both dimensions, 60 $t_1$ increments and 256 points during acquisition. Two hypercomplex 2D data sets were recorded separately and processed using the method described by States et al.[37] In order to confirm that spin diffusion and molecular reorientation due to the thermal motion are insignificant during sample reorientation, the SMAS−DECODER spectrum of melt-spun fibers with a reorientation angle of 360° at the spin rate of 100 Hz was measured. All the signal falls along the diagonal in this case, indicating that both effects may be neglected for mixing times up to 10 ms. In addition, measurements on each sample were repeated with different reorientation angles to confirm the interpretation of the experimental results.

## $^{13}C$ Chemical Shift Tensors for HIQ

Both the magnitude of the principal values and the relative orientation with respect to the molecular struc-

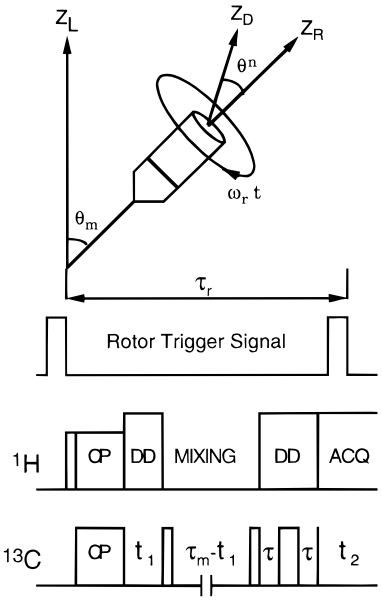


**Figure 2.** Rotor-synchronized pulse sequence of the two-dimensional SMAS−DECODER NMR experiment. $\tau_r$ is the cycle of the rotor period, and $\omega_r$ is the spinning rate. The initial magnetization is created by cross-polarization (CP) and evolves under the proton dipolar decoupling (DD) during the $t_1$ period. The magnetization is stored along the $z$ direction during the mixing time to get a total rotation angle of $\omega_r\tau_m$ with respect to the initial angle. A final spin echo with delay $\tau$ is applied to detect the signal during the $t_2$ acquisition (ACQ) period.

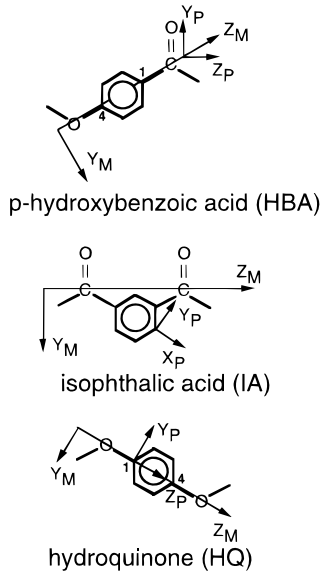


**Figure 3.** Molecular structure of monomers in the HIQ segment. The $z$-axes of the molecular reference frames are defined along the vectors defined by the two atoms bonded to the aromatic ring (C−O in HBA, C−C in IA and O−O in HQ). The orientation of the CSA tensors of the carbon sites in each segment are also shown.

ture of the chemical shift tensor of each carbon site in HIQ are required for the 2D NMR line shape calculation. With regard to the determination of principal values of the chemical shift tensors, the ester carbon in HBA and IA repeat units, the phenylene carbon adjacent to oxygen in HBA (carbon 4 in Figure 3), and the phenylene carbons adjacent to the ester oxygen in HQ (carbons 1 and 4 in Figure 3) are well separated in the CPMAS spectrum of the HIQ polymer samples. The principal values of the chemical shift tensor were determined from measurements of the intensities of spin side bands under different spin speeds, as described by Herzfeld and Berger.[38] The principal values ($\sigma_x$, $\sigma_y$, $\sigma_z$) of the chemical shift tensors, in ppm relative to the TMS standard, were determined to be 244, 127, and 115 for the ester carbon in the HBA and IA repeat units. This is comparable to the measurement of 258, 116, and 116 for the carbonyl group in the homopolymer of HBA by Fyfe.[39,40] Principal values of 236, 126, and 81 were determined for the phenylene 4-carbon in the HBA repeat unit, and 245, 129, and 87 for the phenylene 1,4-carbons in the HQ repeat unit. The remaining phenylene carbons exhibit too much overlap in the polymer spectrum to permit accurate determination of principal values. Instead, for these remaining carbons we have used the values determined by Gérard et al. from CPMAS studies of model compounds.[41]

The relative orientation of the principal axes of the chemical shift tensors for each nuclear site are intrinsic to the local bonding environment about each carbon. Since there are no single-crystal samples of HIQ available, the orientations of the principal axes of each chemical shift tensor on the repeat unit structure are more difficult to determine empirically and must be inferred from NMR studies of model compounds. Studies of the orientation of the principal axes of chemical shift tensors have been reviewed for numerous characteristic molecular architectures.[42] In the case of aromatic and ester carbons, the orientations of the chemical shift tensors are well defined and exhibit little difference from one material to the next (e.g. the most shielded axis is always perpendicular to the $sp^2$ plane). It is possible therefore to define the orientation of the chemical shielding tensor of each carbon site with respect to its local bonding environment with some confidence. For each ester carbon, the unique principal value $\sigma_z$ is that furthest downfield, and corresponds to an axis in the plane of the ester group, perpendicular to the C═O double bond in the direction of the ether oxygen. $\sigma_x$ is the upfield principal value and corresponds to an axis perpendicular to the carboxyl plane. The axis for $\sigma_y$ is always chosen to define a right-handed system. For the phenylene 4-carbon in HBA, and the 1,4-carbons in HQ, the unique principal value $\sigma_z$ is also downfield and corresponds to an axis of the chemical shift tensor which lies along the C−O bond (radial from the ring center). $\sigma_x$ is the upfield principal value and corresponds to an axis perpendicular to the plane of the phenylene ring. For the remainder of the aromatic carbons, the unique principal value $\sigma_z$ is upfield and corresponds to the axis perpendicular to the phenylene ring plane, while $\sigma_x$ is the downfield principal value and corresponds to an axis parallel to the radial direction from the center of the phenylene ring. These axes are illustrated in Figure 3 for representative carbons in the three repeat units.

Interpretation of DECODER results in terms of molecular orientation requires that one invoke some suitable frame of reference for the basic molecular subunits comprising the polymer chain. This choice of molecular subunit is somewhat arbitrary, but reflects a trade-off between the true conformational variability available to the subunits and limitations in the number of degrees of freedom which may be introduced into the analysis with confidence. The subunits should be small enough to be fixed in geometry, at least in approximation, but not so small as to introduce more orientation distributions than can realistically be determined. Unlike the situation with WAXS analysis, however, intermolecular packing considerations may be neglected, and the difficulties attending conformational flexibility may

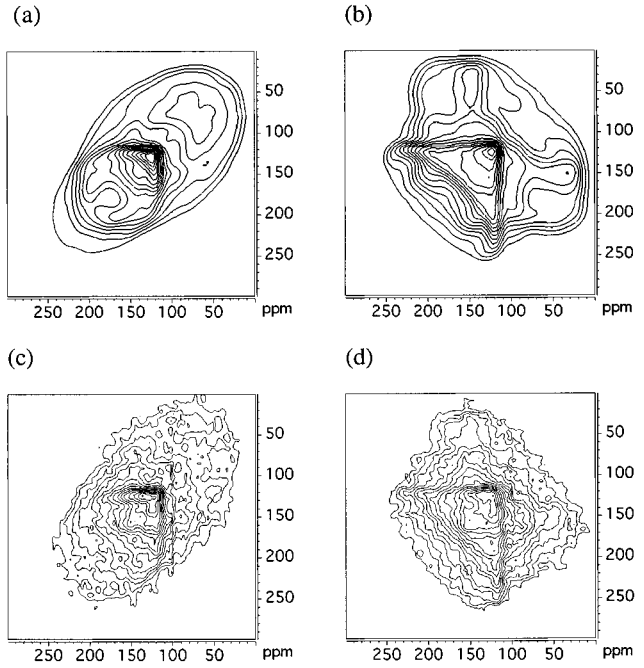


**Figure 4.** Two-dimensional SMAS−DECODER NMR spectra of HIQ powder sample at the spin rate of 100 Hz. (a) simulated spectrum using a reorientation angle of 45°; (b) simulated spectrum using a reorientation angle of 180°; (c) experimental spectrum using a reorientation angle of 45°; (d) experimental spectrum using a reorientation angle of 180°. The simulated spectra are calculated using a uniform orientation distribution function.

be mitigated through selection of appropriately small subunits, without loss of generality. In the light of the "rigidity" of the monomeric units in HIQ polyesters, defining "molecular orientation" as that corresponding to the orientation of unique repeat unit types appears to be the logical choice. This choice overlooks correlations that may exist between successive monomers along the chain and the fact that some sequence combinations are chemically disallowed (e.g. IA−IA or HQ−HQ). However, for the purposes of this analysis, we disregard any such correlation between orientation of different monomer types. The molecular frame of reference MF for each repeat unit is also illustrated in Figure 3, along with the orientation of principal axes of the chemical shift tensors. Once defined, transformation from PAS to MF is straightforward.[43]

## Results and Discussion

Figure 4 shows the two-dimensional SMAS−DECODER NMR spectra for HIQ powder sample using two different angles of reorientation, $\omega_r\tau_m = 45°$ and 180°, at the spin rate of 100 Hz. Both of the experimental spectra (Figure 4c,d) exhibit frequencies broadly distributed over a wide frequency range. Such spectral width offers better sensitivity for determination of orientation distributions. However, both spectra are complicated by considerable spectral overlap between different aromatic carbons, and between aromatic and ester carbons. Nevertheless, all of the spectra exhibit two distinct features. The first is a region of well-defined high intensity (e.g. the triangular-shaped signal in the lower left quadrant of the spectra obtained at 180 degree reorientation angle) corresponding to the 2D line shape assigned collectively to the 1,4-carbon sites on the phenylene ring in the HQ unit, the 1-carbon in the HBA unit, and the ester carbons. The second feature is a more diffuse signal which overlaps the first and is collectively assigned to the remaining carbons in the aromatic rings. The first feature is deemed the more reliable, due both to its better definition in the experimental spectra and to the fact that it was possible to determine the CSA tensors for the carbons of the polymer itself. The characteristic orientation and magnitude of the CSA tensors allow us to determine the molecular orientation both qualitatively and quantitatively. The simulated spectra (Figure 4a,b) are calculated using an isotropic orientation distribution function for each repeat unit. Discrepancies occur in some instances between the simulated and experimental spectra with regard to the second, diffuse feature, but these are relatively minor and may be due to the lack of data on the CSA tensors specific to these remaining aromatic carbons in the polymer sample. Better agreement between the simulated and experimental spectra could be obtained by adjusting the orientation and magnitudes of the CSA tensors associated with these carbons, but the resulting determinations would probably reflect a convolution of uncertainty in the CSA tensors and in the orientation distribution itself. Such refinement was not deemed necessary in the analysis presented here. As an aside, we note that overlap of the anisotropic chemical shift from different carbon sites could be mitigated, in principle, by separation of the individual carbon signals in a third dimension. We conducted preliminary magic-angle-turning experiments,[44,45] combining the SMAS−DECODER experiment with isotropic chemical shift separation in the third dimension in an attempt to resolve individual subspectra. Our results indicate that to some extent overlap can be eliminated for one or more of the carbon species in HIQ but that the desired separation between the phenylene 4-carbon in HBA and the 1,4-carbons in HQ, which are only about 5−6 ppm apart, is impractical.

Figures 5 and 6 illustrate the SMAS−DECODER 2D NMR spectra for HIQ melt-extruded monofilament and melt-spun fiber respectively, again using the same angles of reorientation (45 and 180°) and spin rate (100 Hz). In these cases, the spectra are symmetric along the diagonal due to the uniaxial symmetry of the sample and alignment of the sample symmetry axis parallel to the rotor axis. Visual inspection of the experimental spectra in Figures 5 and 6, and comparison to the powder sample spectra in Figure 4, offers qualitative confirmation of increasing orientation from powder to monofilament to high-speed melt spun fiber. The 2D-NMR line shape feature associated with carbon 4 in the HBA unit, carbons 1 and 4 in the HQ unit, and the ester carbons appears as a narrow band nearly perpendicular to the main diagonal at the highest degree of orientation, shown in Figure 6. Appropriate selection of the reorientation angle during the experiment may be used to minimize the overlap and improve the sensitivity of the orientation distribution analysis. It can be seen that with the HIQ sample axes packed parallel to the rotor axis and using a reorientation angle of 180° rotation, the 2D NMR line shapes are more sensitive to changes in molecular orientation than are those using 45° rotation.

The simulated spectra are calculated using the principal values and relative orientation of the chemical shift tensors described in the previous section with the orientation distribution described by eq 3. In this analysis, we have further simplified the calculation by assuming that the orientation of the main axes of all

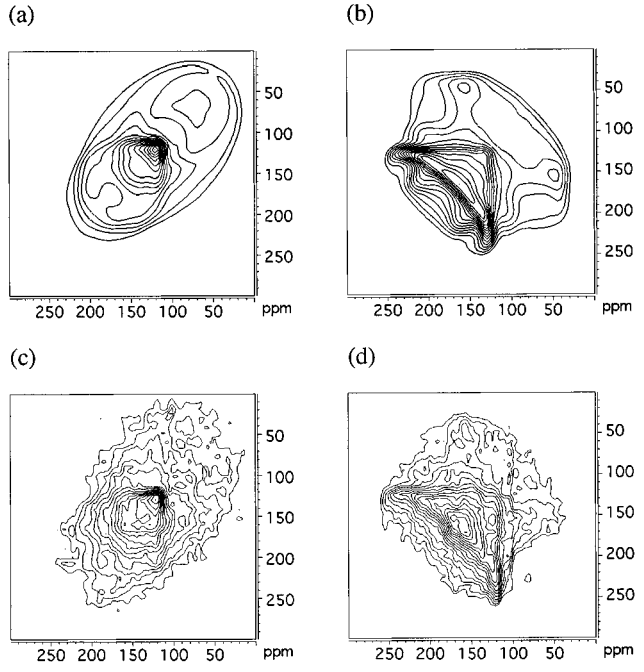


**Figure 5.** Two-dimensional SMAS−DECODER NMR spectra of HIQ melt-extruded monofilament with the sample axis parallel to the rotor axis at the spin rate of 100 Hz: (a) simulated spectrum using a reorientation angle of 45°; (b) simulated spectrum using a reorientation angle of 180°; (c) experimental spectrum using a reorientation angle of 45°; (d) experimental spectrum using a reorientation angle of 180°. The simulated spectra are calculated using an orientation distribution function consisting of a Gaussian component with fwhm of 60° mixed with 20% isotropic distribution.

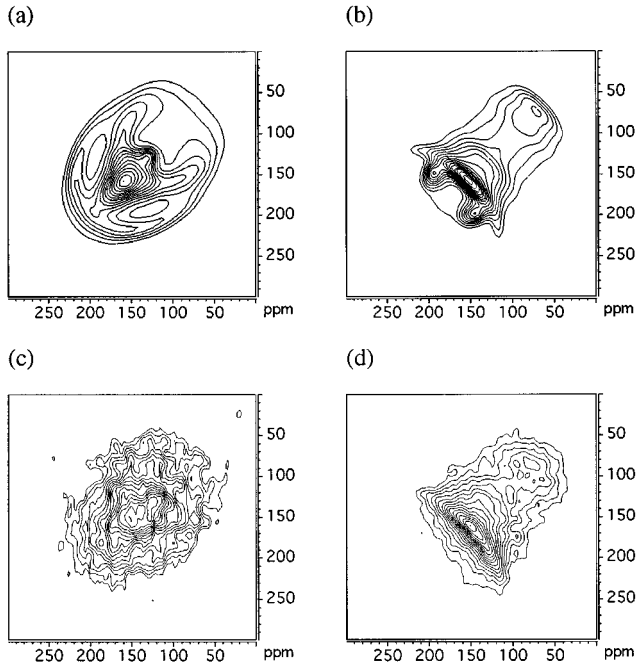


**Figure 6.** Two-dimensional SMAS−DECODER NMR spectra of HIQ melt-spun fiber with the sample axis parallel to the rotor axis at the spin rate of 100 Hz: (a) simulated spectrum using a reorientation angle of 45°; (b) simulated spectrum using a reorientation angle of 180°; (c) experimental spectrum using a reorientation angle of 45°; (d) experimental spectrum using a reorientation angle of 180°. The simulated spectra are calculated using an orientation distribution function consisting of a Gaussian component with fwhm of 20° mixed with 10% isotropic distribution.

three monomer types may be described by the same distribution. This is clearly an approximation, given the

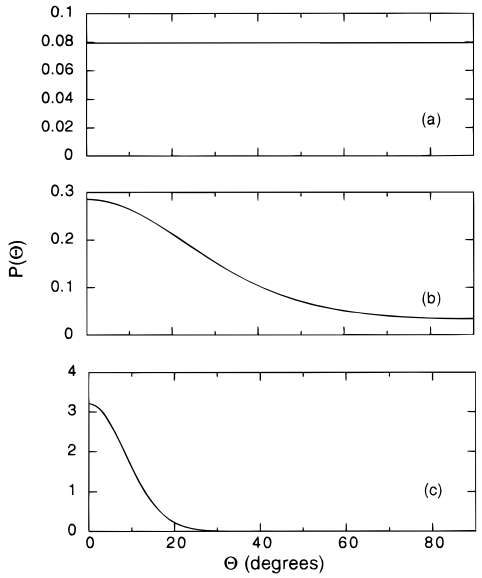


**Figure 7.** Molecular orientation distribution functions $P(\Theta_M)$ for HIQ (a) powder, (b) melt-extruded monofilament, and (c) melt-spun fiber samples. Note the different scalings for the ordinate in each case.

**Table 1. Order Parameter of the Orientation Distribution Function for the Melt-Extruded Monofilament and Melt-Spun Fiber Samples**

| | $P_2$ | $P_4$ | $P_6$ | $P_8$ | $P_{10}$ | $P_{12}$ | $P_{14}$ |
|---|---|---|---|---|---|---|---|
| monofilament | 0.32 | 0.08 | 0.02 | | | | |
| fiber | 0.84 | 0.71 | 0.56 | 0.40 | 0.25 | 0.16 | 0.09 |

structural differences of the IA monomer from HBA and HQ. However, the observation that values of $\Theta_M^0$ significantly different from zero lead to qualitatively different 2D spectra supports the assertion that the definition of MF made here for each repeat unit is consistent with orientation of the *z*-axes of each MF being predominantly along the *z*-axis of the DF and therefore describable by distribution functions which share the same basic features. Best fit for the extruded monofilament, as judged by visual inspection of spectra at different angles of reorientation, was achieved using a distribution function with 80% Gaussian component having fwhm of 60° and 20% isotropic component. In the case of the high-speed melt-spun fiber, an orientation distribution function with 90% Gaussian component having fwhm of 20° and 10% isotropic component provided the best agreement. These are illustrated in parts a and b of Figures 5 and 6, respectively. The primary feature of the spectra, associated with carbon 4 of HBA, carbons 1 and 4 of HQ, and the ester carbons, is well reproduced for each reorientation angle in each sample using the CSA values measured for the polymer and the respective repeat unit orientation distribution function for each sample. Attention to minor discrepancies in the more diffuse feature, which may arise from any of several sources, would not significantly alter our conclusions with regard to the $P(\Theta_M)$ deduced for each sample. The calculated orientation distribution functions of HIQ powder, monofilament and fiber are plotted in Figure 7. The corresponding Legendre coefficients computed from these distribution are listed in Table 1. The results are consistent with a high degree of orientation in the melt-spun fiber, a lesser degree of orientation in the melt-extruded monofilament, and no preferential orientation in the powder sample.

As mentioned earlier, HIQ-35 samples have been studied previously using broad line NMR analysis of the

proton−proton dipolar coupling in fiber and tape samples at temperatures ranging from 198 to 413 K.[20] In that work, the second moment $\langle \Delta H^2 \rangle$ of the frequency distribution was measured as a function of sample orientation in the magnetic field to yield values of $A_n$ for $n =$ 0, 2, and 4 in the following equations:

$$\langle \Delta \mathrm{H}^2 \rangle = A_0 P_0 + A_2 P_2(\cos \beta) + A_4 P_4(\cos \beta) \quad (7)$$

$$A_n = \frac{4 c_\mathrm{n} G}{N} \sum_{j<k} \frac{\mathrm{P_n}(\cos \Theta_{jk})}{r_{jk}^{\,6}} \quad (8)$$

$\beta$ is the orientation of the sample director with respect to the magnetic field and $\Theta_{jk}$ is the orientation of the vector from proton j to proton k with respect to the sample director. $G = 895.4$ G$^2$ Å$^6$ for protons, and $c_n$ is a prefactor with values of $^1/_5$, $^2/_7$, and $^{18}/_{35}$ for $n = 0$, 2, and 4, respectively.[46] $N$ is the number of protons. In broad line NMR measurements at 298 K of annealed HIQ fibers similar to those used here, values of $A_0 =$ 4.6, $A_2 = 1.5$, and $A_4 = 1.6$ were reported.[20] Contact with those measurements may be made by the following approximate analysis.

Since contributions to eq 8 fall off as $r_{\mathrm{hh}}{}^{-6}$, where $r_{\mathrm{hh}}$ is the distance between protons, it suffices to consider only the protons bonded to adjacent carbons in each repeat unit for the intramolecular contribution to the second moment. As is evident from Figure 4 of ref 20, there are also significant intermolecular proton−proton interactions, but these appear to be distributed in an approximately isotropic manner and contribute only to a vertical shift of the second moment anisotropy curve with increasing temperature. Assuming that each repeat unit in the polymer is oriented with transverse isotropy about the sample axis and invoking the Legendre addition theorem, $\langle P_n(\cos \Theta_{jk}) \rangle$ may be rewritten as $\langle P_n(\cos \beta_{\mathrm{p},jk}) \rangle P_n(\cos \Theta_\mathrm{M})$, where $\beta_{\mathrm{p},jk}$ is the orientation of the $jk$th proton−proton vector in the MF. For HBA, HQ and IA, the value of $\beta_{\mathrm{p},jk}$ is 0, 0, and 30°, respectively. Bond distances are taken to be 1.39 and 1.10 Å for the C−C and C−H bonds, respectively. With this simple model, one obtains values of 0.80 and 0.61 for $P_2$ and $P_4$, respectively. The second Legendre coefficient for those fibers is in very good agreement with that measured by SMAS−DECODER for the annealed fibers used in this work. The fourth coefficient is slightly lower, consistent with the greater uncertainly in estimation of the higher order coefficient. Values of $P_2$ and $P_4$ equal to 0.84 and 0.64, respectively, were obtained by Johnson et al. for HIQ fibers of comparable composition, using WAXS analysis of equatorial reflections.[15] In that case, the authors argued for an orientation distribution of rodlike sections of HBA and HQ of various lengths connected by IA "joints". Significantly, the coefficient series does not appear to be converged by $n = 4$, suggesting that higher order terms would be required to reconstruct the full orientation distribution in these cases.

## Conclusion

We have applied the SMAS−DECODER method to determine the molecular orientation in samples of a main chain thermotropic liquid crystal polyester processed under several different conditions. Full orientation distribution functions for the repeat units comprising the terpolyester were deduced from the calculated SMAS−DECODER spectra. A purely isotropic distribution was sufficient to characterize the powder sample. For oriented monofilament and fiber samples, a simple model comprising a Gaussian component with a process-dependent full width at half-maximum (fwhm) mixed with some fraction of isotropic component was invoked. Both the fraction of oriented component and the degree of orientation increased with the higher shear conditions of the fiber spinning process.

The SMAS−DECODER method provides a reliable and reasonably sensitive measurement of the molecular scale orientation. Even in situations as complicated as the present one where several different monomer types, each possessing several different carbon sites, are present and the principal values and the orientation of the chemical shift tensor are not precisely known, the calculated NMR line shapes show qualitatively consistent results in the determination of orientation distributions of the monomeric units when compared with the experimental data. The resulting orientation distributions provide accurate, molecular level information about the alignment of chemical constituents under different process conditions. The method is quantitative even without isotopic enrichment, and therefore it is applicable to studies of industrial production processes.

**Acknowledgment.** We are grateful to Professors H. W. Spiess, K. Schmidt-Rohr, and K. K. Gleason for helpful suggestions on the NMR experiments and to D. C. Oda for many enlightening discussions. We also wish to express our appreciation to Professor U. W. Suter for making ref 31 available in advance of publication. The samples employed in this work were made available to us by Hoechst-Celanese and the University of Leeds. Financial support for this work was provided by the NSF through a Young Investigator award to GCR (CTS-9457111).

## References and Notes

(1) Ward, I. M. *Mechanical Properties of Solid Polymers,* 2nd ed.; John Wiley & Sons: New York, 1983.
(2) Ward, I. M. *Developments in Oriented Polymers—II,* ; Elsevier Applied Science: New York, 1987.
(3) Erdemir, A. B.; Johnson, D. J.; Tomka, J. G. *Polymer* **1986**, *27,* 441.
(4) Erdemir, A. B.; Johnson, D. J.; Karacan, I.; Tomka, J. G. *Polymer* **1988**, *29,* 597.
(5) Hsiao, B. S.; Shaw, M. T.; Samulski, E. T. *Macromolecules* **1988**, *21,* 543.
(6) Hsiao, B. S.; Shaw, M. T.; Samulski, E. T. *J. Polym. Sci.: Part B: Polym. Phys.* **1990**, *28,* 189.
(7) Kiss, G. J. *J. Rheol.* **1986**, *30,* 585.
(8) Blundell, D. J.; McDonald, W. A.; Chivers, R. A. *High Perform. Polym.* **1989**, *1* (2), 97.
(9) Brown, P. J.; Karacan, I.; McIntyre, J. E.; Milburn, A. H.; Tomka, J. G. *Polym. Int.* **1991**, *24,* 23.
(10) Viney, C.; Mitchell, G. R.; Windle, A. H. *Mol. Cryst. Liq. Cryst.* **1985**, *129,* 75.
(11) Windle, A. H. In *Developments in Oriented Polymers—I*; Ward, I. M., Ed.; Elsevier Applied Science: New York, 1982; Chapter 1.
(12) Schmidt-Rohr, K.; Spiess, H. W. *Multidimensional Solid-State NMR and Polymers*; Academic Press: San Diego, CA, 1994.
(13) Windle, A. H.; Viney, C.; Golombok, R.; Donald, A. M.; Mitchell, G. R. *Faraday Discuss. Chem. Soc.* **1985**, *79,* 55.
(14) Blundell, D. J.; Chivers, R. A.; Curson, A. D.; Love, J. C.; McDonald, W. A. *Polymer* **1988**, *29,* 1459.
(15) Johnson, D. J.; Karacan, I.; Tomka, J. G. *Polymer* **1991**, *32,* 2312.
(16) Blackwell, J.; Biswas, A.; Gutierrez, G. A.; Chivers, R. A. *Faraday Discuss. Chem. Soc.* **1985**, *79,* 73.
(17) Mitchell, G. R.; Windle, A. H. In *Developments in Crystalline Polymers —II*; Bassett, D. C., Ed.; Elsevier Applied Science: New York, 1988; Chapter 3, p 115.
(18) McBrierty, V. J.; Ward, I. M. *J. Phys.* **1968**, *D1,* 1529.
(19) Allen, R. A.; Ward, I. M. *Polymer* **1991**, *32,* 202.

(20) Rutledge, G. C.; Ward, I. M. *J. Polym. Sci.: Part B: Polym. Phys.* **1993**, *31*, 513.
(21) Hentschel, R.; Schlitter, J.; Sillescu, H.; Spiess, H. W. *J. Chem. Phys.* **1978**, *68*, 56.
(22) Hentschel, R.; Sillescu, H.; Spiess, H. W. *Polymer* **1981**, *22*, 1516.
(23) Spiess, H. W. In *Developments in Oriented Polymers—I*; Ward, I. M., Ed., Elsevier Applied Science: New York, 1982; Chapter 2.
(24) Kulik, A. S.; Spiess, H. W. *Macromol. Chem. Phys.* **1994**, *195*, 1755.
(25) Utz, M.; Tomaselli, M.; Ernst, R. R.; Suter, U. W. *Macromolecules* **1996**, *29*, 2909.
(26) Harbison, G. S.; Spiess, H. W. *Chem. Phys. Lett.* **1986**, *124*, 128.
(27) Harbison, G. S.; Vogt, V.-D.; Spiess, H. W. *J. Chem. Phys.* **1987**, *86*, 1206.
(28) Henrichs, P. M. *Macromolecules* **1987**, *20*, 2099.
(29) Schmidt-Rohr, K.; Hehn, M.; Schaefer, D.; Spiess, H. W. *J. Chem. Phys.* **1992**, *4*, 2247.
(30) Chmelka, B. F.; Schmidt-Rohr, K.; Spiess, H. W. *Macromolecules* **1993**, *26*, 2282.
(31) Utz, M.; Eisenegger, J.; Suter, U. W.; Ernst, R. R. *J. Magn. Reson.*, in press.
(32) Lewis, R. H.; Long, H. W.; Schmidt-Rohr, K.; Spiess, H. W. *J. Magn. Reson.* **1995**, *115A*, 26.
(33) Haeberlen, U. *High Resolution NMR in Solids (Advances in Magnetic Resonance, Supplement 1)*; Academic Press: New York, 1976.
(34) Mehring, M. *High Resolution NMR in Solids*, 2nd ed.; Springer-Verlag: Berlin, 1983.
(35) Veeman, W. S. *Prog. NMR Spectrosc.* **1984**, *16*, 193.
(36) Bower, D. I. *J. Polym. Sci., Part B: Polym. Phys.* **1981**, *19*, 93.
(37) States, D. J.; Haberkorn, R. A.; Ruben, D. J. *J. Magn. Reson.* **1982**, *48*, 286.
(38) Herzfeld, J.; Berger, A. *J. Chem. Phys.* **1980**, *73*, 6021.
(39) Fyfe, C. A.; Lyerla, J. R.; Volksen, W.; Yannoni, C. S. *Macromolecules* **1979**, *12*, 757.
(40) Lyerla, J. R.; Economy, J.; Maresch, G. G.; Muhlebach, A.; Yannoni, C. S.; Fyfe, C. A. In *Liquid Crystalline Polymer*; Weiss, R. A., Ober, C. K., Eds.; American Chemical Society: Washington, DC, 1990; Chapter 25.
(41) Gérard, A.; Lauprêtre, F.; Monnerie, L. *Macromolecules* **1993**, *26*, 3313.
(42) Ernst, R. R.; Bodenhausen, G.; Wokaun, A. *Principles of Nuclear Magnetic Resonance in One and Two Dimensions*; Clarendon Press: Oxford, England, 1987.
(43) Rose, M. E. *Elementary Theory of Angular Momentum*; John Wiley and Sons: New York, 1957.
(44) Hu, J. Z.; Wang, W.; Liu, F.; Solum, M. S.; Alderman, D. W.; Pugmire, R. J.; Grant, D. M. *J. Magn. Reson.* **1995**, *113A*, 210.
(45) Gan, Z. *J. Am. Chem. Soc.* **1992**, *114*, 8307.
(46) McBrierty, V. J.; Ward, I. M. *Br. J. Appl. Phys. (J. Phys. D)* **1968**, *2* (1), 1529.

MA970927S